Biocompatible Poly(lactic acid)-Based Hybrid Piezoelectric and Electret Nanogenerator for Electronic Skin Applications

Shaobo Gong, Bowen Zhang, Jinxi Zhang, Zhong Lin Wang,* and Kailiang Ren*

Human machine interface (HMI) devices, which can convert human motions to electrical signals to control/charge electronic devices, have attracted tremendous attention from the engineering and science fields. Herein, the high output voltage from a nonpiezoelectric *meso*-poly(lactic acid) (*meso*-PLA) electret-based triboelectric nanogenerator (NG) is combined with the relatively high current from a double-layered poly(L-lactic acid) (PLLA)-based piezoelectric nanogenerator (PENG) for an E-skin (electronic skin) (HMI) device application. The hybrid NG with a cantilever structure can generate an output voltage of 70 V and a current of 25 μA at the resonance frequency of 19.7 Hz and a tip load of 4.71 g. Moreover, the output power of the hybrid NG reaches 0.31 mW, which is 11% higher than that from the PLLA-based PENG. Furthermore, it is demonstrated that the PLA-based hybrid NG can be used to turn a light-emitting diode light on and off through an energy management circuit during a bending test. Finally, it is demonstrated that the PLA-based woven E-skin device can generate the output signals of 35 V (V_{oc}) and 1 μA (I_{sc}) during an elbow bending test. The advantages of biocompatible, ease of fabrication, and relatively high output power in the hybrid NG device show great promise for future E-skin applications.

1. Introduction

With the rapid development of personal electronic devices and the Internet of Things (IoT), human machine interface (HMI)

S. Gong, Dr. B. Zhang, Dr. J. Zhang, Prof. Z. L. Wang, Prof. K. Ren
Beijing Key Laboratory of Micro-Nano Energy and Sensor
CAS Center for Excellence in Nanoscience
Beijing Institute of Nanoenergy and Nanosystems
Chinese Academy of Sciences
Beijing 100083, China
E-mail: zlwang@binn.cas.cn; renkailiang@binn.cas.cn
S. Gong
College of Materials Science and Opto-Electronic Technology
University of Chinese Academy of Science
Beijing 100049, China
Prof. Z. L. Wang, Prof. K. Ren
Center on Nanoenergy Research
School of Physical Science and Technology Guangxi University
Nanning, Guangxi 530004, China
Prof. Z. L. Wang
School of Materials Science and Engineering
Georgia Institute of Technology
Atlanta, GA 30332, USA

The ORCID identification number(s) for the author(s) of this article can be found under https://doi.org/10.1002/adfm.201908724.

devices that connect people with electronic devices have gained widespread scientific and engineering attention.[1–3] Currently, wearable smart fabrics (also called electronic skins), which can convert human motions to electric signals and use these signals to control/charge portable electronics, have been the subject of intensive research.[4–6] Recently, various types of E-skin devices have been exploited based on a variety of working principles, including piezoresistive,[7,8] capacitive,[9,10] piezoelectric,[11,12] and electrostatic effects.[13–15] Compared with other E-skin devices, electrostatic and piezoelectric based E-skin devices hold great promise in future HMI devices due to several advantages, including their ease of fabrication, high sensitivity, and self-powered properties.

Since being first developed in 1950s, electret material has been broadly employed in many applications, including transducers, microphones, electrostatic recordings, and energy harvesting devices.[16–21] The polarity of electret materials mainly results from charged air bubbles or space charges injected by a corona charger at a high DC voltage, which performs as electric dipoles appearing piezoelectricity. Thus, a poly(tetrafluoroethylene) (PTFE) based polymer electret normally exhibits a piezoelectric coefficient d_{33} of 200 pC N^{-1}, which is much larger than that for most piezoelectric polymers.

Recently, a tremendous research effort has been devoted to developing electronic skin using the triboelectric nanogenerator (TENG) effect.[13] In 2017, Pu et al. investigated a very high bond (VHB) (acrylate polymers, VHB 184, 3M) and an ionic hydrogel-based stretchable TENG for electronic skin applications, which show an ultrahigh stretchability and an output power of 35 mW cm^{-3}, demonstrating its potential in E-skin applications.[22] Recently, we demonstrated that a monocharged electret nanogenerator (NG) can generate an output voltage of ≈170 V, which can be used for wearable energy harvesting and pressure sensor applications.[23,24] Previous publications also indicated that the coupling of friction charges and injected charges in electret materials are beneficial to enhancing electrostatic induction.[16,25] Therefore, in this investigation, we plan to combine electret nanogenerators with triboelectric nanogenerators for E-skin applications.

In 2006, Ren et al. studied energy harvesting applications using a 1–3 lead magnesium niobate -lead titanate/epoxy

ADVANCED
SCIENCE NEWS
www.advancedsciencenews.com

ADVANCED
FUNCTIONAL
MATERIALS
www.afm-journal.de

composite that exhibited an energy density of 22 mW cm^{-3} at a stress of 44 MPa.[26] This was the first time that a single crystal based 1–3 composite was used for energy harvesting applications. Later, Yuan et al. presented a poly(vinylidene fluoride) (PVDF)/ZnO based composite for E-skin application, which successfully detected human elbow movement with high sensitivity.[6] However, most piezoceramic nanogenerator devices are not environmentally friendly, especially lead zirconate titanate ceramics. Compared with those of piezoceramics, piezoelectric polymers show high flexibility and good impedance matching with environment. Thus, they become the preferred material for E-skin applications.

As the most widely used piezoelectric polymers, PVDF shows the largest piezoelectricity among piezoelectric polymers.[27] However, the pyroelectric property of PVDF makes it possible to detect temperature signals, which may be confused with a pressure signal in E-skin applications. As one of widely used piezoelectric polymers, poly(L-lactic acid) (PLLA) is synthesized by the polymerization of L-lactic acid monomers and it can be used for applications of actuators, smart fabric, and filtration devices.[28–30] The piezoelectric polymer PLLA features a large number of C=O double bonds with an angle of 125° relative to the main carbon chain, and the parallel dipole component of the C=O dipoles can show polarity under shear stress.[31,32] Additionally, the molecular structure of a stretched PLLA polymer possesses a β form crystal conformation with a 3_1 helical structure, which contributes to the great thermal stability and large piezoelectricity of the PLLA material. Moreover, PLLA exhibits nonpyroelectricity, which is critical for distinguishing pressure signals from thermal signals in E-skin applications. In 2017, our group investigated a biodegradable PLLA piezoelectric polymer for energy harvesting application, which possessed an output power of 10 µW cm^{-2} and had an excellent thermal stability at 140 °C for 24 h.[32]

Similarly with PLLA, meso-PLA (poly(lactic acid)) is synthesized by the polymerization of meso-lactide. Due to the presence of both levo and dextral helical structures, meso-PLA normally shows nonpiezoelectricity.[33] Because lactide can be derived from plenty of renewable sources, including corn and rice, meso-PLA shows the property of biodegradability and biocompatibility. It is known that a meso-PLA based electret material can keep injected space charges for more than a few months or even longer.[34] Even though its surface potential is lower than that of a PTFE electret film, its biocompatibility and biodegradability enable us to use this material for hybrid nanogenerator applications (E-TENG and piezoelectric nanogenerator (PENG)). In addition, the biodegradability of PLA based materials have been intensively studied by previous researchers.[35,36] PLLA polymer can slowly degrade in soil and completely degrade with proteinase K at 37 °C and pancreatic lipase at 55 °C. However, since PLA material is relatively stable in air, the degradation of PLA has no significant effect on device performance. Thus, in this investigation, we combined the high voltage from an electret based nanogenerator and the relatively high current from a PLLA piezoelectric nanogenerator. Next, the hybrid NG was utilized to successfully transmit and receive an infrared signal through a lab-designed wireless infrared sensing system. Furthermore, the hybrid NG was woven into a wearable fabric device, which was utilized to detect human elbow movement. During an elbow bending test, the output voltage and the short circuit current of the hybrid NG were 35 V and 1 µA, respectively. The hybrid NG showed great promise for a suitable material to fabricate biodegradable E-skin applications.

2. Device Design and Working Mechanism

2.1. Structural Design of the Hybrid Nanogenerator

As shown in **Figure 1**a, the hybrid NG device consists of two PENGs located in the top and bottom of the device, respectively. In the device, a double-layered electret based triboelectric nanogenerator is located in the middle of the device. The PENG device consists of a unimorph structure in which the double-layered PLLA films are the active layers and nonpiezoelectric meso-PLA films are the passive layer. In the E-TENG device, two corona charged meso-PLA films are hot pressed together with a triangular waveform structure. Au electrodes are sputter coated on the bottom and top of the PENG devices as induction electrodes for the E-TENG device.

2.2. Theoretical Analysis

Figure 1c shows the charge distribution of the electret-based TENG (E-TENG) in its initial state. Generally, the charges inside a meso-PLA electret film (σ_0) can be divided into two types. One type consists of space charges injected into the meso-PLA film during a corona charging process, which is relatively deep and stable in the film; the other type consists of surface charges produced from the triboelectric effect between the meso-PLA and the Au electrode during the working process. Due to the electro potential difference between the Au electrode and the meso-PLA film, electrons will spontaneously flow between them to be kept in a potential well found in the shallow surface layer of the film.[37] The surface charge can only be kept for a relatively short time in the surface layer of an electret.

In this investigation, the induced charges in the E-TENG are assumed to distribute uniformly on the induction electrode and metal electrode (the sputter coated Au electrode on the film) of the electret. Here, the induced charge densities on the induction electrode and the metal electrode of the electret are set as σ_{i1} and σ_{i2}, respectively. From Gauss's law, the equation is set as follows

$$2k\sigma_{i1} + \sigma_{i2} = -2\sigma_0 \tag{1}$$

In a certain position x, the induced charge density can be expressed as[23,24]

$$\sigma_x = -\frac{\sigma_0}{2k\left(1 + \varepsilon_r \dfrac{2xh}{t_0 l_0}\right)} \tag{2}$$

where σ_x is the induced charge density at a certain point x, ε_r is the relative permittivity of the meso-PLA electret, t_0 is the
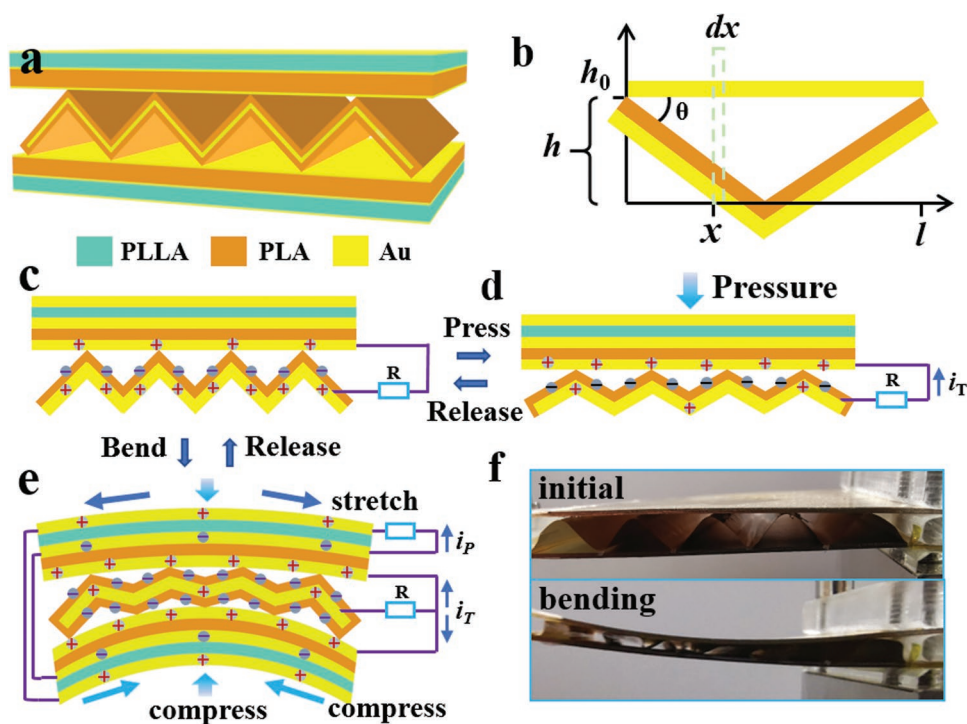
Figure 1. Schematic diagram and working mechanism of the hybrid nanogenerator (NG): a) Schematic diagram of the hybrid NG. b) Enlarged schematic drawing of the E-TENG device with a triangle waveform. c) Schematic diagram of charge distribution for the hybrid NG in its initial state, d) compression mode, and e) bending mode. f) Photographs of the initial and bending state of the hybrid NG.

thickness of the *meso*-PLA film, h and l_0 are the height and the wavelength of the triangle wave structure of the meso-PLA electret.

As shown in Figure 1b, k is set as $k = l_0 / \sqrt{4h_0^2 + l_0^2}$, where h_0 the original height of the triangle wave structure of the meso-PLA electret and k is the length ratio between the induction electrode and the PLA electret.

Thus, the induced charge density on the induction electrode can be expressed as

$$\sigma_{i1} = \overline{\sigma_x} = \frac{\int_0^{l/2} \sigma_x \, dx}{l/2} = -\frac{t_0 \sigma_0}{2k\varepsilon_r h} \ln\left(1 + \frac{\varepsilon_r h}{t_0}\right) \quad (3)$$

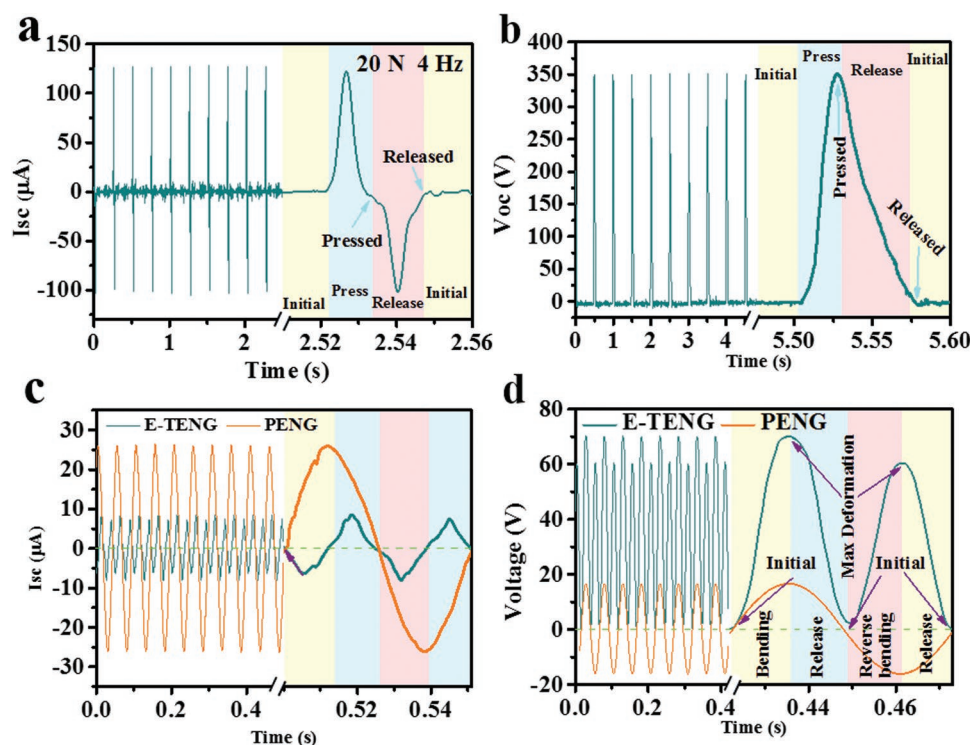In Equation (3), $h \gg t_0$, $\sigma_0 < 0$, so we can obtain the following equation

$$\frac{\partial \sigma_{i1}}{\partial h} < 0 \quad (4)$$

During this investigation, Equations (2) and (3) are used to theoretically analyze how the induced charges on the top induction electrode will change with the height of the triangular waveform structure. For a certain shape of the triangle waveform structure, the ratio between the height and wavelength of the triangle waveform structure is constant. From the simulation result using Equation (3) in Figure S1b in the Supporting Information, the induced charges increase with the decrease of the height of the triangular waveform structure.

2.3. Working Principle of the Hybrid NG

In this investigation, the hybrid NG has two basic working modes. As shown in Figure 1c,d, one of them is the compression mode. From Equations (3) and (4), when the hybrid NG is compressed, the induced charges on the induction electrode of the E-TENG device will increase due to the decreasing distance between the induction electrode and the electret film. Simultaneously, the induced charges on the metal electrode of the electret will decrease to maintain a charge balance between them. As a result, the current will flow from the metal electrode of the electret film to the induction electrode. Conversely, when the pressure is released, the increasing induction distance can generate a current in the opposite direction. However, during the compression test, due to the triangular shape of the E-TENG device, the compression force was mostly loaded on the TENG device. Therefore, the PENG device exhibited a very weak output voltage. Thus, the hybrid nanogenerator exhibited similar output performance with that of the TENG. Thus, the output signal of the PENG was ignored at the compression test.

If the device is designed as a cantilever structure, the device will mostly work in a bending mode. A schematic drawing of the cantilever structure is shown in Figure S3 in the Supporting Information. Photos of the device in the initial and bending states are shown in Figure 1f, indicating the varied induction distance. This means that the E-TENG device can generate current flow during the bending mode. Moreover, as shown in Figure 1e, due to the bending of the *meso*-PLA film in a unimorph structure, the PLLA film on the upper substrate is

**ADVANCED
SCIENCE NEWS**
www.advancedsciencenews.com

**ADVANCED
FUNCTIONAL
MATERIALS**
www.afm-journal.de

Figure 2. Compression test of the hybrid NG: a) short circuit current and b) open circuit voltage. Bending test of the hybrid NG: c) short-circuit current and d) open-circuit voltage.

stretched, inducing a tensile stress along the shear direction. In addition, the PLLA film on the bottom part of the hybrid nanogenerator is subjected to a compression stress, resulting in its dipoles having opposite changes. Thus, the PENG device will also functionize in this process.

To verify the working principle of the hybrid NG at two different working modes, the hybrid NG device was measured, and the result is shown in **Figure 2** at different modes. For the compression mode, the output signals of the device at a periodic pulse pressure are shown in Figure 2a,b. As analyzed previously, the E-TENG device works in this mode. In the beginning, when a compression stress is applied on the device, the E-TENG can generate a positive current in the external circuit (from the metal electrode of the electret to the top induction electrode) and cause a voltage rise owing to the increasing pressure. Conversely, when the device is released, the output voltage of the device decreases, causing a reverse current (from the induction electrodes to the metal electrode). In the last step, the E-TENG device returns to its initial state when the pressure is completely removed.

For the bending mode, as analyzed in the previous paragraph, both the E-TENG and the PENG device will functionalize in this mode. The data shown in Figure 2c,d are the measurement data for the short circuit current and open circuit voltage from the hybrid NG device in the bending mode. First, the bending of the hybrid NG generates a tensile stress on the top PLLA unimorph and a compression stress on the bottom of the unimorph structure. Then, both the E-TENG and PENG generate a positive voltage and current. Afterward, the release process of the hybrid NG increases the induction distance of
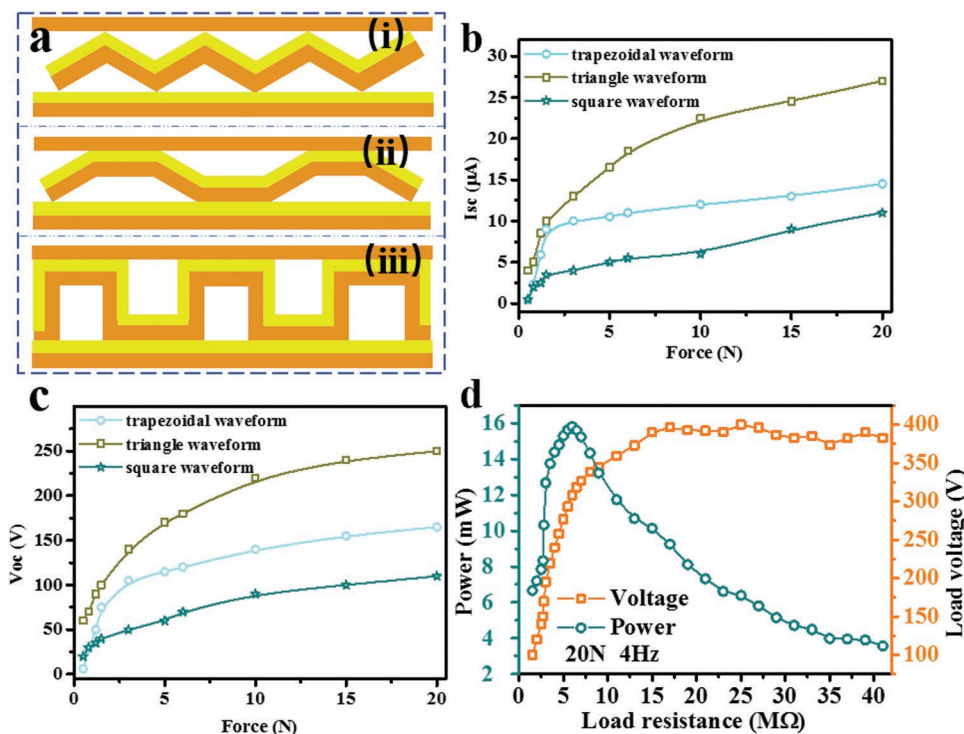
E-TENG, generating a reverse current and a voltage drop in the external circuit. In the equilibrium position, there is no deformation in the hybrid NG. Thus, both the output voltages of the E-TENG and the PENG are zero. Afterward, as the hybrid NG is bent in reverse, the E-TENG undergoes the same compression stress, which will generate the same current and voltage as previously explained. However, due to the opposite direction of the stress, the PENG will produce a reverse current and an opposite voltage. It is worth noting that the E-TENG undergoes two repeated processes in one bending cycle, causing the frequency of the output signal of the E-TENG to be twice that of the PENG.

3. Results and Discussion

3.1. Compression Test of the E-TENG

To improve the output performance of the E-TENG, the device was designed with a *meso*-PLA based electret film with various shapes, including a triangular waveform, trapezoidal waveform, and square waveform. The schematic drawings of the device design are shown in **Figure 3**a.

The output performance of the three E-TENG devices with various structures was measured. Because the data shown in Figure 3b,c are for a comparison purpose, all three E-TENG with various structures were measured at a frequency of 2 Hz. As the data shown in Figure 3b,c, the short circuit currents (I_{sc}) of the E-TENG devices increase with increasing pressure. Among them, the square-waveform E-TENG device exhibits the lowest

**ADVANCED
SCIENCE NEWS**
www.advancedsciencenews.com

**ADVANCED
FUNCTIONAL
MATERIALS**
www.afm-journal.de

Figure 3. Compression test of the E-TENG device: a) Schematic drawing of the single-layered *meso*-PLA electret-based E-TENG device with various waveforms: i) triangular waveform, ii) trapezoidal waveform, and iii) rectangular waveform. Force dependence of b) short circuit current and c) open circuit voltage of E-TENG with various structures at 2 Hz. d) Load resistance dependence of the output voltage and output power of the E-TENG at a pulse force of 20 N and 4 Hz frequency.

short circuit current at the same pressure as the others. This may mainly arise from its stiff structure in the vertical direction of the device. However, the triangle-waveform E-TENG device exhibits the largest open circuit voltage and short circuit current at the same pressure. At a pressure of 20 N, the short-circuit current of the triangle-waveform E-TENG device is 27 µA, which is almost 2.5 times that of the square-waveform E-TENG device. Moreover, the maximum open-circuit voltage of 250 V is 2.27 times that of the square-waveform E-TENG. Originally, the triangle waveform TENG was designed with a shape of an ideal triangle waveform as the schematic drawing shown in Figure 3a. However, after a few bending cycles, it becomes round shape as shown in Figure 1f due to the relatively soft structure in the E-TENG structure. Among these three TENG devices with various structures, the trapezoidal waveform E-TENG has the smallest electret area, which limits its output performance. Although the square waveform E-TENG has the largest induction area, but its stiff structure cause a lower deformation, resulting in a lower output energy density. Compared with other two waveform structures, the triangular waveform E-TENG has a relatively large electret area and the largest deformation of the electret membrane at the same pressure as compared with the others. Consequently, the triangular E-TENG exhibited the largest output performance. Therefore, the triangle waveform E-TENG is adopted in this research.

Moreover, to increase the output current of the E-TENG device, two layers of the *meso*-PLA films are glued together with an Au electrode as the common electrode in the middle of the E-TENG device. In the following studies, this double-layered

meso-PLA based electret is used as the basic material for the E-TENG device. To simplify the expression, the double-layered *meso*-PLA electret-based TENG device with a triangle waveform is referred to as the E-TENG in the following discussion.

Because the E-TENG can generate a higher current at a higher frequency and the frequency limitation for the Linmotor system is below 4 Hz, the output power density of the E-TENG were measured at 4 Hz to achieve a higher output power density of the device. The load resistance dependence of the output voltage and output power of the E-TENG were measured at a pressure of 20 N at 4 Hz. The data shown in Figure 3d indicate that the output voltage increases with increasing load resistance and finally reaches a maximum value of ≈390 V. With a matching resistor of 6 MΩ, the maximum output power is 15.81 mW. Previously, we proposed that a shoe insole nanogenerator can generate an output power density of 1.48 µW cm^{-3}. During this investigation, the dimension of the E-TENG is 5 cm (l) *4. 5 (w) * 0.5 (t) and the calculated power density of the E-TENG device is 1.41 mW cm^{-3}, which is much larger than the previous results.[23] This may be the result of the increasing electret area for the E-TENG device with a triangle-waveform structure relative to that of a plain surface electret. In addition, It demonstrates that an increasing electret area is beneficial to the output power of the electret device.

3.2. Bending Test of the Hybrid NG

To study the output performance of the hybrid NG in the bending mode, a theoretical analysis of the cantilever beam

**ADVANCED
SCIENCE NEWS**

www.advancedsciencenews.com

**ADVANCED
FUNCTIONAL
MATERIALS**

www.afm-journal.de

is used to predict the bending deformation of the hybrid NG, and a schematic diagram of the experimental setup is shown in Figure S3 in the Supporting Information. In this investigation, the length of the piezoelectric PLLA film is set at 5 cm. From our previous publication, it is known that the thickness ratio between the active layer (PLLA film in this investigation) and passive layer plays a critical role in the performance of a unimorph device.[39] However, in this application, to maintain the flexibility of a wearable device, a double layer of the PLLA film is used as the active layer in the unimorph structure of the hybrid NG. Thus, only the effect of the tip load and the excitation signal frequency are studied for the performance of the hybrid NG.

3.2.1. Bending Test of the Single-Layered PLLA-Based PENG (SL-PENG)

To study the effect of the resonance frequency and tip load on the performance of the cantilever beam, a SL-PENG was measured. First, as shown in Figure S4b in the Supporting Information, the short circuit current and open circuit voltage of the SL-PENG reached a maximum at the resonance frequency. In addition, the resonance frequency of the SL-PENG decreases with increasing tip load. From the data shown in Figure S4c in the Supporting Information, the output power initially increases with increasing tip loads due to an increase of the input mechanical energy. After the tip load exceeds 4.7 g, the output power of the device starts to decrease. This may arise from the reduced electromechanical conversion efficiency of the device with increasing tip load. The maximum output power and corresponding resonant frequency of the SL-PENG device as a function of tip load are summarized in **Figure 4**c. From the data, the optimized tip load and the resonant frequency are 4.71 g and 19.1 Hz, respectively. As shown in Figure S4e in the Supporting Information, the output voltage increases with the load resistance at the resonant frequency, and it starts to saturate after the load resistor is larger than 3 MΩ. The maximum output power of the SL-PENG is 0.14 mW at a load resistance of 1.1 MΩ.

In the PENG device, the electric potential of the PENG is set as U, so the output voltage and power can be expressed as

$$P = \frac{V_{Load}^2}{R} = \frac{U^2}{\left(\sqrt{R} + \dfrac{r}{\sqrt{R}}\right)^2} \tag{5}$$
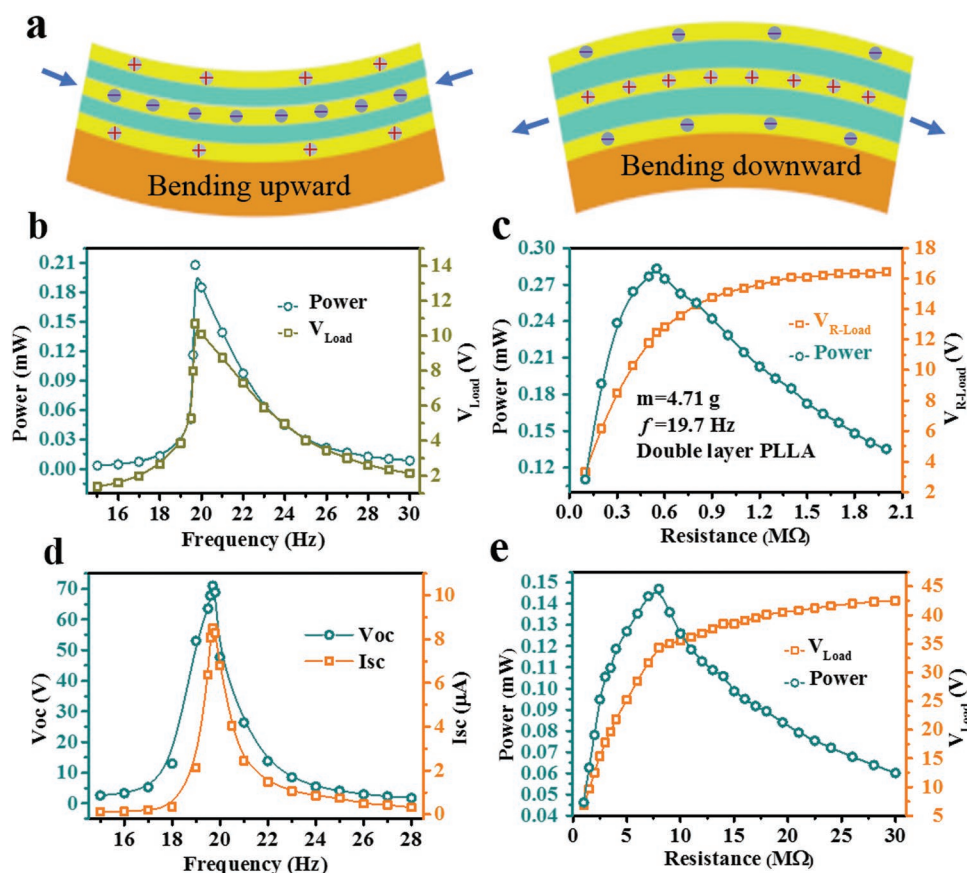
Figure 4. Bending test of hybrid NG. For the double-layered PENG (DL-PENG): a) Working mechanism of the DL-PENG device. b) Frequency dependence of the output voltage and corresponding output power of the DL-PENG at a tip load of 4.71 g. c) Load resistance dependence of the output voltage and corresponding output power of the DL-PENG at a resonance frequency of 19.7 Hz and a tip load of 4.71 g. For the E-TENG device: d) Frequency dependence of the short-circuit current and open-circuit voltage of the E-TENG at a tip load of 4.71 g. e) Load resistance dependence of the output voltage and corresponding output power of the E-TENG at a resonance frequency of 19.7 Hz and a tip load of 4.71 g.

1908724 (6 of 11)

**ADVANCED
SCIENCE NEWS**
www.advancedsciencenews.com

**ADVANCED
FUNCTIONAL
MATERIALS**
www.afm-journal.de

where r is the internal resistance of the PENG and R is the load resistance. From Equation (5), if the load resistance is equal to the internal impedance of the device, the output power reaches the maximum value of P_{max} ($P_{max} = U^2/4r$).[29] In this situation, as the load result is equal to 1.1 MΩ, the output power of the device reaches its maximum value.

3.2.2. Bending Test of the Double-Layered PLLA-Based PENG (DL-PENG)

From previous literature, it is also known that a multilayer piezoelectric material exhibited multiple times improvement in piezoelectric coefficient than that of the single layer piezoelectric material,[38] which can generate a much larger output signal than that of the single layer material during energy harvesting applications. Our previous results also demonstrated that if the active layers and passive layers have similar Young's modulus, the best performance of the cantilever device can be achieved if they have equal thickness.[39] In this application, our research aim was focused on a wearable electronic skin application and a thick PLLA layer can increase the stiffness of the wearable E-skin device. Thus in this investigation, we only focus on the PLLA film with double layers. Additionally, to improve the input mechanical energy, a *meso*-PLA film with a thickness of 0.5 mm was used as a passive layer. As shown in Figure 4a, the double layers of the PLLA film were bonded together by a hot pressing method using a thin Au electrode in the middle as a common electrode. Since the weight of the PLLA film is much smaller than that of the tip load, the influence of the second PLLA layer on the resonance frequency and the optimized tip load of the device is ignored. Therefore, the tip load used in the following study was fixed at 4.71 g. At the optimized tip load and resonant frequency, the bending movement of the PLLA/PLA cantilever was measured by a high speed camera and the measured displacement was 15.5 mm. Subsequently, the radius of PLLA/PLA cantilever was calculated by the equation presented in our previous publication.[39] The calculated radius and curvature of the cantilever were 27.42 cm and 3.65 cm^{-1}, respectively. As shown in Figure S4f in the Supporting Information, the open circuit voltage of DL-PENG at the resonant frequency is 16.9 V, which is similar to that for the SL-PENG device. However, the short-circuit current of the DL-PENG is 26.7 µA, which is approximately two times that of the SL-PENG. Furthermore, the output voltage and power of the DL-PENG device as a function of frequency in a range from 15 to 30 Hz was measured, and the data are shown in Figure 4c. The data indicate that the resonance frequency slightly fluctuates to 19.7 Hz for the DL-PENG devices. Next, the output power of the DL-PENG was measured as a function of load resistance with the optimized tip load at the resonance frequency. From the data shown in Figure 4c, the measured matching resistance is 0.55 MΩ, which is half of the value for the SL-PENG device. Additionally, the maximum output power at the matching resistance is 0.28 mW, which is twice that of SL-PENG. The increasing power of the PENG may mainly arise from the enlarged capacitance of the DL-PENG device compared with that of the SL-PENG device. In summary, it demonstrated that a double-layered PLLA structure effectively improves the output power of a cantilever-structured PENG device.
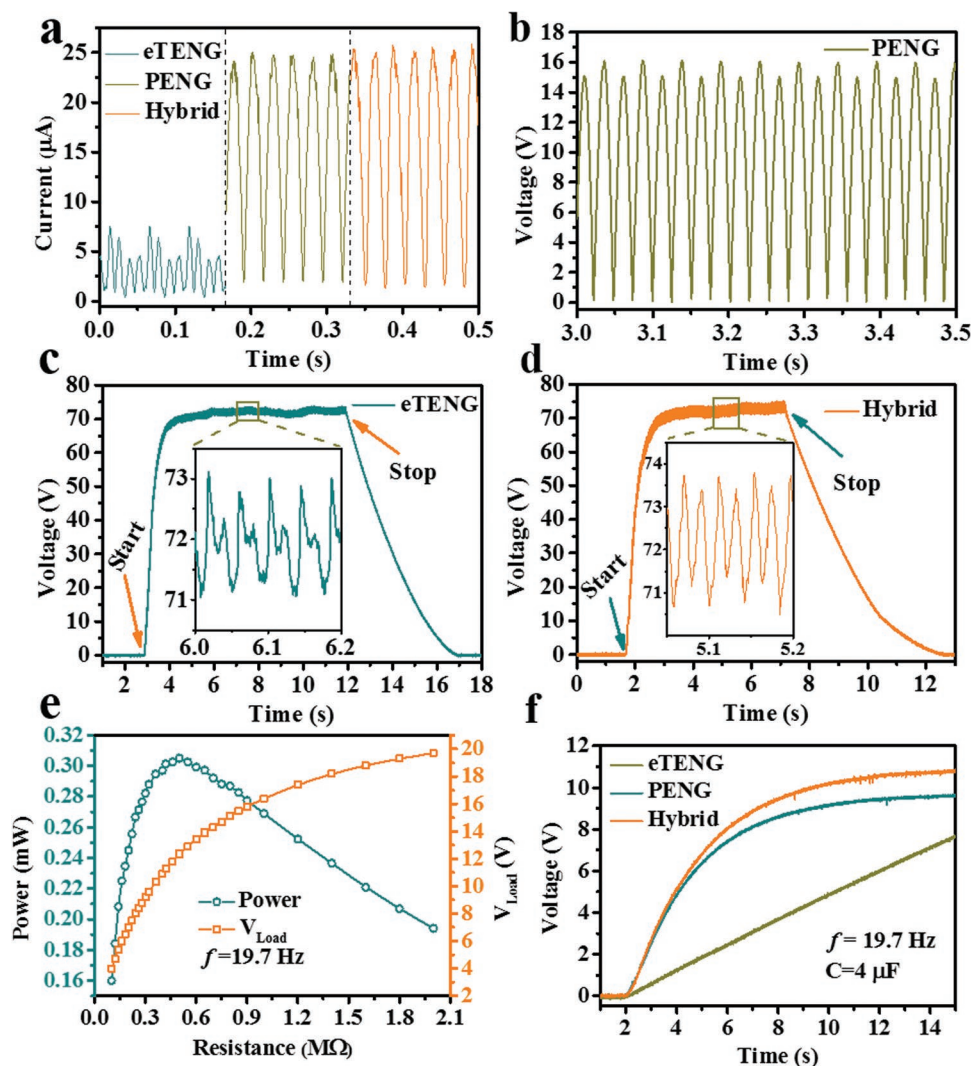
3.2.3. Bending Test of the E-TENG

Since the optimized tip load and resonance frequency of the PENG have been determined, these parameters were also used to measure the output performance of the E-TENG device. The frequency dependence of the open-circuit voltage and short-circuit current of the E-TENG were measured and the data are shown in Figure 4d. The data indicate that the maximum open circuit voltage and short circuit current of the E-TENG at the resonant frequency reached 71 V and 8.5 µA, respectively. Furthermore, the load resistance dependence of the output voltage and power were measured at the resonance frequency (19.7 Hz) and the data are shown in Figure 4e. The data demonstrate that the maximum output power reaches 0.147 mW at a matching resistance of 8 MΩ. However, the output power of the E-TENG device in the bending mode is much smaller than that generated from the compression mode. This may be attributed to the lower deformation of the E-TENG device in the bending mode.

3.3. Measurement of the Hybrid NG

From the testing result, it is concluded that the E-TENG presents a relatively high output voltage and a small current, while the PENG presents a relatively large current and low voltage. To take advantage of the different structures of the device, the output signals of the E-TENG and PENG were individually rectified by a full-wave rectification circuit and then connected together in series to power electronic devices. Additionally, the rectified signal from all three nanogenerators was measured in the bending mode using the rectified circuit. From the data shown in **Figure 5**a, it is found that the current of the hybrid NG (25.7 µA) is slightly larger than the current of the PENG (25 µA). As shown in Figure 5c, the output voltage of the E-TENG (72 V) fluctuates around the average value of 72 V with an amplitude of 1.7 V. Similar to the data shown in Figure 5d, the rectified voltage of the hybrid NG fluctuates ≈72 V with an amplitude of ≈3 V. In this situation, the fluctuation in the output voltage in the hybrid NG could mainly come from the different working frequency of the PENG with the E-TENG. Therefore, the hybrid NG combines both advantages of high output voltage from the E-TENG and a relatively high current from the PENG. As shown in Figure 5e, the output power of the hybrid NG reaches a maximum value of 0.31 mW at a matching resistance of 0.5 MΩ, which is 11% higher than that of the PENG. However, in this situation, the output power of the E-TENG only exhibited a small power of 0.03 mW due to the difference in the matching resistance between the TENG (8 MΩ) and the PENG (0.55 MΩ). This can be solved by using an impedance matching circuit in the future hybrid device. Additionally, in an arm bending test for E-skin, the E-TENG may exhibit much larger output signals than that of the PENG. Therefore, the hybrid nanogenerator show greater advantages than the PENG device in the device performance.

**ADVANCED
SCIENCE NEWS**
www.advancedsciencenews.com

**ADVANCED
FUNCTIONAL
MATERIALS**
www.afm-journal.de

Figure 5. Output performance of the hybrid NG: a) Short-circuit current of the E-TENG, the PENG, and the hybrid NG. Open-circuit voltage of the b) PENG, c) E-TENG, and d) hybrid NG. e) Output voltage and corresponding output power of the hybrid NG as a function of load resistance at the resonance frequency of 19.7 Hz and a tip load of 4.71 g. f) Capacitance charging curve for all the nanogenerators, in which a 4 µF capacitor was charged.

In addition, the reliability is another important parameter to evaluate the operating life of the device. To demonstrate that, the durability of the hybrid NG was tested in the bending mode for more than 10 000 working cycles at a resonance frequency of 19.7 Hz. The output voltage of the PENG was measured with the matching resistance for the TENG and PENG, respectively. As the data shown in Figure S5a in the Supporting Information, the output voltage of the PENG decreased by 5.8% after 10 000 working cycles. The enlarged view of the output voltage of the PENG after 10 000 working cycles is shown in Figure S5b in the Supporting Information. Similarly, according to the data shown in Figure S5c,d in the Supporting Information, the output voltage of the E-TENG decreased by 5.8% after 10 000 working cycles. The decrease in the output voltage of the E-TENG mainly attributes to the crack in the Au electrode of the E-TENG device, which may result from the difference in Young's modulus between the PLA and the Au layer in the E-TENG device. However, the Au electrode can be replaced by a

flexible conductive electrode in the future device. These measurement results demonstrate the high reliability of the hybrid NG.

4. Applications of the Hybrid NG

To power an electronic device, an energy management circuit (EMC) is necessary to modulate the output of the hybrid NG to increase the output current and reduce the output voltage of the nanogenerator. In this investigation, the EMC circuit employed for this application is an LTC3588 (Analog Devices Inc., Mansfield Texas, USA). A photograph and an equivalent circuit of the EMC circuit and the IR sensing system are shown in Figure S6a,b in the Supporting Information, respectively. During the circuit working process, the output energy of the hybrid NG continuously accumulated in the EMC, and the infrared receiver was in the off state. Once the voltage of
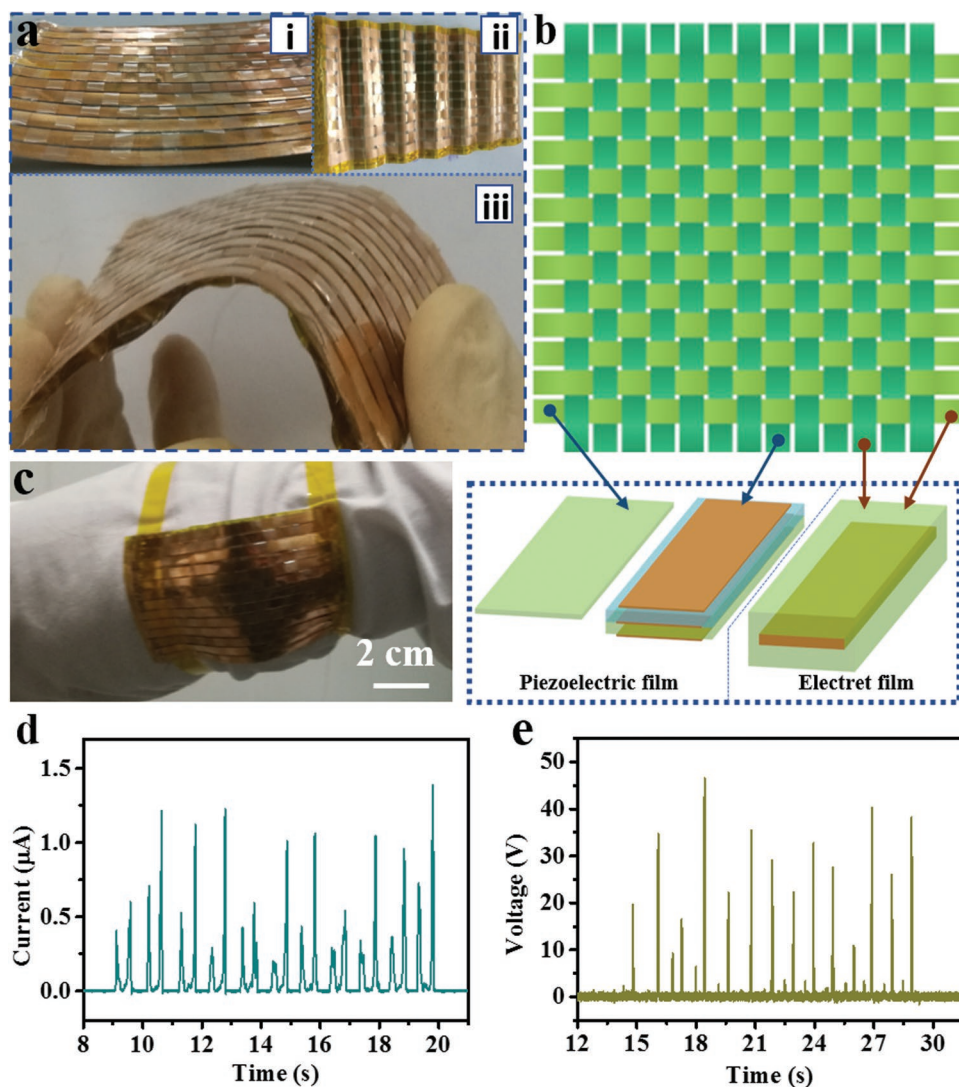
Figure 6. Biocompatible woven E-skin device: a) Photographs of i) woven PENG, ii) woven E-TENG, and iii) woven-hybrid NG. b) Schematic drawing of the woven PENG and E-TENG. c) Picture of the woven-hybrid NG during the elbow testing. d) The measurement results of the short-circuit current and e) open-circuit voltage of the woven hybrid NG during the elbow test.

the EMC reached 3.6 V, the EMC instantly released a certain amount of power to drive the infrared emitter in the circuit using an infrared signal. Instantly, the infrared receiver was triggered and switched from the off state to the on state and lit an light-emitting diode (LED) in the circuit. The Video S1 in the Supporting Information clearly presents this working process. The output voltage of the EMC and the IR receiver were measured by a Keithley 6514 electrometer, and the data are shown in Figure S6c,d in the Supporting Information. The data indicate that the signals from the transmitter and the receiver are exactly the same frequency with a spacing of 0.53 s. This demonstrated that the infrared sensor was powered from the hybrid NG through the EMC circuit.

Next, the hybrid NG was used to power a calculator for a demonstration purpose. As shown in Figure S6e in the Supporting Information, when the cantilever of the hybrid NG begins to vibrate, the output voltage of the EMC gradually rises to ≈3 V, and then, the calculator lights up. Figure S6f in the

Supporting Information shows that the output voltage of the EMC fluctuates between 3.45 and 3.54 V, which can constantly supply the required power for the calculator. Detailed information on this process is shown in Video S2 in the Supporting Information.

Finally, a wearable hybrid NG was fabricated using a weaving ribbons method for E-skin application, which can convert human motions into electrical signals to control portable electronic devices. Photographs of the woven PENG, the woven triangular-waveform E-TENG and the bending hybrid NG are shown in **Figure 6**ai–iii, respectively. As the schematic diagram shown in Figure 6b, the wearable E-skin NG was fabricated by woven ribbons along both the horizontal and vertical directions. In the woven NG, the E-TENG was fabricated into a ribbon with a *meso*-PLA/Au/*meso*-PLA structure. However, the woven PENG has a structure of nonpiezoelectric *meso*-PLA ribbons along the horizontal direction as the supporting frame of the wearable E-skin and a PLLA/*meso*-PLA unimorph (active layer) structure

along the vertical direction as the function material. During the test, as shown in Figure 6c, the wearable hybrid NG was tightly attached on a human elbow for the measurement. The testing results are shown in Figure 6d,e, with output signals of 35 V (V_{oc}) and 1 μA (I_{sc}) generated during the elbow bending test. Detailed information on the elbow testing process is shown in Videos S3 and S4 in the Supporting Information. This experimental result demonstrates that the hybrid NG can be used as a wearable E-skin for remote control applications. In this investigation, the hybrid NG and woven wearable device were fabricated using all biocompatible PLA based materials, including meso-PLA electret film, and piezoelectric polymer PLLA. Due to the properties of thermal stability in PLLA film and charge stability on meso-PLA electret film, the hybrid NG shows an excellent stability on the device performance. The advantages of biocompatibility, device stability, and relatively high output power in the hybrid NG device provide great promise for future E-skin applications.

5. Conclusion

In this investigation, we proposed a biocompatible hybrid nanogenerator comprising a piezoelectric PLLA film and a meso-PLA electret-based triboelectric nanogenerator. First, in a compression-recovery mode, the E-TENG exhibited an output power density of 7 W m^{-2} at a matching resistance of 6 MΩ and a maximum power density of 65.3 mW m^{-2} in the bending mode. Furthermore, we combined the high output voltage from a non-piezoelectric meso-poly(lactic acid) (meso-PLA) electret-based triboelectric nanogenerator and the relatively high current from a double-layered PLLA-based PENG for application in an E-skin (electronic skin) HMI device. The biocompatible hybrid NG can generate an output voltage of 70 V and a current of 25 μA at the resonance frequency of 19.7 Hz and a tip load of 4.71 g. Moreover, the output power of the hybrid NG reached 0.31 mW, which was 11% higher than that from the PLLA-based PENG. Furthermore, we demonstrated that the PLA-based hybrid NG can be used to turn an LED light on and off through an energy management circuit during a bending test. Finally, it was demonstrated that the PLA-based woven E-skin device can generate the output signals of 35 V (V_{oc}) and 1 μA (I_{sc}) during an elbow bending test. The advantages of biocompatibility, device stability, and relatively high output power in the hybrid NG device provide great promise for future E-skin applications.

6. Experimental Section

Fabrication of the Double-Layered PLLA Film: As shown in Figure S7 in the Supporting Information, to prepare the PLLA film in the PENG, PLLA powders (M_W = 260 000, polydispersity index ≤1, Sigma-Aldrich Corp., USA) were dissolved in dichloromethane and stirred for 4 h at room temperature to obtain a uniform solution. Next, the prepared uniform solution was cast on a clean steel plate and dried at room temperature for 24 h to completely evaporate the solvent. Then, the PLLA film was peeled off the steel plate and uniaxially stretched four times using a lab-designed zone stretching machine. After annealing in an oven at 135 °C for 4 h, the stretched film was cut into a rectangular shape with dimensions of 4 cm (width) × 5 cm (length) along a 45° angle relative

to the stretching direction, and the rectangular PLLA film was sputter coated with Au on one side. Afterward, two Au coated PLLA films were hot pressed together for a structure of PLLA/Au/PLLA/Au using a hot press machine (TY608-8T, Tianyu Machinery Equipment Co. LTD, Zhejiang, China) with a pressure of 8 MPa at 155 °C for 30 min. Finally, an Au electrode was sputter coated on the top layer of the double-layered PLLA film as the electrode for the PENG device.

Fabrication of the E-TENG and Hybrid NG: To prepare the meso-PLA-based electret film, as shown in Figure S7 in the Supporting Information, two PLA films with a thickness of 10 μm were first prepared by a solution casting method as described in the previous paragraph. Next, one of the meso-PLA films was sputter coated with Au on one side and the two layers of meso-PLA film were hot pressed together with the Au electrode in the middle. Finally, the double-layered meso-PLA film was hot pressed in a designed triangular wave mold at 50 °C for 30 min to form a triangular-waveform structure. Next, the meso-PLA electret film was charged by a corona charger at 15 kV of DC voltage and a grid voltage of 3 kV. After that, the PLLA film based PENG devices were taped on the top and bottom of the triangle waveform-structured E-TENG device. Finally, the wires were connected to complete the fabrication of the hybrid NG, as shown in Figure 1e.

Fabrication of the Wearable E-Skin: First, the double-layered PLLA piezoelectric film was cut into strips of 3 mm wide and adhered to 3 mm wide strips of the nonpiezoelectric meso-PLA film (passive layer, 50 μm) using double-sided tape. Next, a gold electrode was sputtered on the bottom of the meso-PLA passive layer to form a unimorph structure for the PENG. Afterward, the strips of the unimorph-structured PENG and the meso-PLA strips were woven together as the warp and weft yarns of a woven PENG cloth as shown in Figure 6b.

Similarly, for the wearable E-TENG device, the double-layered meso-PLA based electret films were cut into strips 3 mm wide and woven as shown in Figure 6b, to form a woven electret film. The woven electret film was hot pressed at 50 °C in a triangle waveform mold to obtain a wearable triangle-waveform E-TENG device. Finally, two woven PENG films were adhered to the top and bottom of the wearable E-TENG device with double-sided tape to obtain the woven E-skin devices. Informed consent was obtained from the volunteer for the bending experiments.

Data Acquisition: In the compression mode, the force was produced by a lab-designed linear motor system (E1100, Linmot USA Inc., USA). In the bending mode, the device was held by a holder on the top of a shaker (VT-20, YMC Piezotronics Inc., Yanghzou, China), as shown in the schematic drawing of the experimental setup in Figure S3 in the Supporting Information. In the bending test, a signal was generated from a functional generator (DS345, Stanford Research Systems, Sunnyvale, USA) to drive a shaker through a power amplifier (Xli202, Crown Audio Inc., Elkhart, USA). All electrical signals of the devices were measured using a Keithley electrometer (6514A, Tektronix Inc., Beaverton, OR, USA).

Supporting Information

Supporting Information is available from the Wiley Online Library or from the author.

Conflict of Interest

The authors declare no conflict of interest.

Keywords

[1] S. Lim, D. Son, J. Kim, Y. B. Lee, J. K. Song, S. Choi, D. J. Lee, J. H. Kim, M. Lee, T. Hyeon, D. H. Kim, *Adv. Funct. Mater.* **2015**, *25*, 375.

[2] X. Q. Liao, W. T. Song, X. Y. Zhang, H. Huang, Y. T. Wang, Y. J. Zheng, *J. Mater. Chem. C* **2018**, *6*, 12841.

[3] A. D. Greer, P. M. Newhook, G. R. Sutherland, *IEEE/ASME Trans. Mechatronics* **2008**, *13*, 355.

[4] B. Xu, A. Akhtar, Y. Liu, H. Chen, W. Yeo, S. Park, B. Boyce, H. Kim, J. Yu, H. Lai, S. Jung, Y. Zhou, J. Kim, S. Cho, Y. Huang, T. Bretl, J. A. Rogers, *Adv. Mater.* **2016**, *28*, 4462.

[5] Q. Z. Zhong, J. Zhong, X. Cheng, X. Yao, B. Wang, W. Li, N. Wu, K. Liu, B. Hu, J. Zhou, *Adv. Mater.* **2015**, *27*, 7130.

[6] H. Yuan, T. M. Lei, Y. Qin, R. S. Yang, *Nano Energy* **2019**, *59*, 84.

[7] N. N. Jason, M. D. Ho, W. L. Cheng, *J. Mater. Chem. C* **2017**, *5*, 5845.

[8] M. J. Ha, S. D. Lim, J. Park, D. S. Um, Y. Lee, H. Ko, *Adv. Funct. Mater.* **2015**, *25*, 2841.

[9] X. Guo, Y. Huang, X. Cai, C. Liu, P. Liu, *Meas. Sci. Technol.* **2016**, *27*, 045105.

[10] S. P. Dai, S. Wang, H. Yan, J. Xu, H. W. Hu, J. N. Ding, N. Y. Yuan, *Mater. Res. Express* **2019**, *6*, 0850b9.

[11] Y. C. Mao, P. Zhao, G. McConohy, H. Yang, Y. X. Tong, X. D. Wang, *Adv. Energy Mater.* **2014**, *4*, 1301624.

[12] H. X. He, Y. M. Fu, W. L. Zang, Q. Wang, L. L. Xing, Y. Zhang, X. Y. Xue, *Nano Energy* **2017**, *31*, 37.

[13] M. Y. Ma, Z. Zhang, Q. L. Liao, F. Yi, L. H. Han, G. J. Zhang, S. Liu, X. Q. Liao, Y. Zhang, *Nano Energy* **2017**, *32*, 389.

[14] H. He, H. Zeng, Y. Fu, W. Han, Y. Dai, L. Xing, Y. Zhang, X. Xue, *J. Mater. Chem. C* **2018**, *6*, 9624.

[15] Y. Dai, Y. Fu, H. Zeng, L. Xing, Y. Zhang, Y. Zhan, X. Xue, *Adv. Funct. Mater.* **2018**, *28*, 1800275.

[16] S. H. Wang, Y. N. Xie, S. M. Niu, L. Lin, C. Liu, Y. S. Zhou, Z. L. Wang, *Adv. Mater.* **2014**, *26*, 6720.

[17] J. W. Zhong, Q. Z. Zhong, G. J. Chen, B. Hu, S. Zhao, X. Li, N. Wu, W. B. Li, H. M. Yu, J. Zhou, *Energy Environ. Sci.* **2016**, *9*, 3085.

[18] G. M. Sessler, *Electrets (Topics in Applied Physics)*, Springer-Verlag, Berlin, Germany **1987**.

[19] G. Sessler, J. West, *J. Acoust. Soc. Am.* **1973**, *53*, 1589.

[20] G. Sessler, J. West, *J. Acoust. Soc. Am.* **1962**, *34*, 1787.

[21] G. Sessler, J. West, *J. Acoust. Soc. Am.* **1966**, *40*, 1434.

[22] X. Pu, M. M. Liu, X. Y. Chen, J. M. Sun, C. H. Du, Y. Zhang, J. Y. Zhai, W. G. Hu, Z. L. Wang, *Sci. Adv.* **2017**, *3*, e1700015.

[23] S. Gong, C. Wang, J. Zhang, C. Zhang, J. E. West, K. Ren, *Adv. Sustainable Syst.* **2018**, *2*, 1700178.

[24] S. Gong, J. Zhang, C. Wang, K. Ren, Z. L. Wang, *Adv. Funct. Mater.* **2019**, *29*, 1807618.

[25] T. Zhou, L. M. Zhang, F. Xue, W. Tang, C. Zhang, Z. L. Wang, *Nano Res.* **2016**, *9*, 1442.

[26] K. Ren, Y. Liu, X. Geng, H. F. Hofmann, Q. M. Zhang, *IEEE Trans. Ultrason., Ferroelectr. Freq. Control* **2006**, *53*, 631.

[27] Y. Fu, H. He, T. Zhao, Y. Dai, W. Han, J. Ma, L. Xing, Y. Zhang, X. Xue, *Nano-Micro Lett.* **2018**, *10*, 76.

[28] Y. Inuzuka, K. Onishi, S. Kinoshita, Y. Nakashima, T. Nagata, H. Yamane, T. Nakai, T. Kataoka, S. Ito, Y. Tajitsu, *Jpn. J. Appl. Phys.* **2012**, *51*, 09LD15.

[29] Y. Tajitsu, *Ferroelectrics* **2016**, *499*, 36.

[30] J. Zhang, S. Gong, C. Wang, D. Y. Jeong, Z. L. Wang, K. Ren, *Macromol. Mater. Eng.* **2019**, *304*, 1900259.

[31] G. R. Zhao, B. S. Huang, J. X. Zhang, A. C. Wang, K. Ren, Z. L. Wang, *Macromol. Mater. Eng.* **2017**, *302*, 1600476.

[32] C. L. Zhao, J. Zhang, Z. L. Wang, K. Ren, *Adv. Sustainable Syst.* **2017**, *1*, 1700068.

[33] D. N. Ghista, *Biomedical Science, Engineering and Technology*, IntechOpen, London, UK **2012**.

[34] X. Gao, L. Huang, B. Wang, D. F. Xu, J. W. Zhong, Z. M. Hu, L. N. Zhang, J. Zhou, *ACS Appl. Mater. Interfaces* **2016**, *8*, 35587.

[35] T. M. Quynh, H. Mitomo, N. Nagasawa, Y. Wada, F. Yoshii, M. Tamada, *Eur. Polym. J.* **2007**, *43*, 1779.

[36] Y. Tokiwa, A. Jarerat, *Biotechnol. Lett.* **2004**, *26*, 771.

[37] R. Hinchet, A. Ghaffarinejad, Y. Lu, J. Yavand Hasani, S. W. Kim, P. Basset, *Nano Energy*, **2018**, *47*, 401.

[38] Q. M. Wang, L. E. Cross, *Appl. Phys. Lett.* **1998**, *72*, 2238.

[39] K. Ren, R. S. Bortolin, Q. M. Zhang, *Appl. Phys. Lett.* **2016**, *108*, 062901.